JOURNAL OF MATERIALS SCIENCE **40** (2005) 3129–3135

High temperature plastic flow and grain boundary chemistry in oxide ceramics

H. YOSHIDA*
National Institute for Materials Science, 1-2-1 Tsukuba, Sengen, Ibaraki 305-0047, Japan
E-mail: YOSHIDA.Hidehiro@nims.go.jp

A. KUWABARA
Department of Materials Science and Engineering, Kyoto University, Yoshida-Honmachi, Sakyo-ku, Kyoto 606-8501, Japan

T. YAMAMOTO
Department of Advanced Materials Science, School of Frontier Science, The University of Tokyo, 7-3-1 Hongo, Bunkyo-ku, Tokyo 113-8656, Japan

Y. IKUHARA
Institution of Engineering Innovation, School of Engineering, The University of Tokyo, 2-11-16 Yayoi, Bunkyo-ku, Tokyo 113-8656, Japan

T. SAKUMA
National Institute for Academic Degrees and University Evaluation, 1-29-1 Gakuennishimachi, Kodaira, 187-8587, Japan

High temperature plastic flow or grain boundary failure in oxide ceramics such as Al_2O_3 and tetragonal ZrO_2 polycrystal (TZP) is sensitive to small levels of doping by various cations. For example, high temperature creep deformation in fine-grained, polycrystalline Al_2O_3 is highly suppressed by 0.1 mol% lanthanoid oxide or ZrO_2-doping. An elongation to failure in superplastic TZP is improved by 0.2–3 mol% GeO_2-doping. A high-resolution transmission electron microscopy (HRTEM) observation and an energy-dispersive X-ray spectroscopy (EDS) analysis revealed that the dopant cations tend to segregate along the grain boundaries in Al_2O_3 and TZP. The dopant effect is attributed to change in the grain boundary diffusivity due to the grain boundary segregation of the dopant cations. A molecular orbital calculation suggests that ionicity is one of the most important parameters to determine the high temperature flow stress, and probably, the grain boundary diffusivity in the oxide ceramics.

1. Introduction

High temperature creep or plastic flow in high-purity, polycrystalline oxide ceramics such as Al_2O_3 and tetragonal ZrO_2 polycrystal (TZP) is often rate-controlled by diffusional process over a wide range of temperatures and strain rates because of limited dislocation movement [1]. Recently, it has been pointed out that the high temperature plastic flow in Al_2O_3 and TZP is very sensitive to small levels of doping by various cations [2–11]. For instance, small amount of ZrO_2-doping is a major reason for improvement of high temperature creep resistance in ZrO_2-added Al_2O_3; the creep deformation in fine-grained Al_2O_3 is highly suppressed by 0.1 mol% ZrO_2-doping as well as 10 wt% (7 vol%) ZrO_2 addition [4]. On the other hand, an elongation to failure in 5 wt%SiO_2-added TZP is remarkably affected by 1000 ppm Li_2O-doping into the glass; the elongation is reduced from 1100% in TZP-5 wt% SiO_2 to only 38% in TZP-5 wt% (SiO_2-2 wt%Li_2O) [7]. Origin of the dopant effect on the high temperature plastic flow cannot be understood from the phenomenological approach based on the constitutive equation, which describes the empirical relationship between strain rate, flow stress and grain size [1]. Therefore, it is necessary to establish an atomistic approach to elucidate the high temperature plastic flow in ceramics. The present paper aims to briefly summarize our recent experimental data of the dopant effect on the high temperature plastic flow in Al_2O_3 and TZP, and to show that change in chemistry of grain boundaries is responsible for the dopant effect. Analysis of the grain boundary chemistry appears one of the useful approaches to describe the grain boundary diffusion in fine-grained oxide ceramics.

*Author to whom all correspondence should be addressed.

2. Experimental procedure

2.1. Sample preparation

In order to investigate the dopant effect in Al_2O_3 and TZP, high-purity Al_2O_3, 3 mol% Y_2O_3 stabilized TZP (3Y-TZP) and high-purity dopant cations' acetates or oxides were used as starting materials. The dopants used were lanthanoid acetate, strontium acetate, fine-grained titanium oxide, germanium oxide, barium oxide, neodymium oxide, colloidal silica and colloidal zirconia. The Al_2O_3 or 3Y-TZP powders and the dopants were ball-milled in ethanol for 24 h. The green compacts of isostatically pressed powders were sintered at 1300–1550°C for 2–4 h in air.

2.2. High temperature mechanical test

High temperature creep experiments were carried out under uniaxial compression in air using a lever-arm testing machine with a resistance-heated furnace. The applied stress and temperature were 20–100 MPa and 1250–1300°C, respectively. High temperature tensile tests were carried out under uniaxial tension in air at a constant cross-head speed using an Instron-type testing machine equipped with a resistance-heated furnace. The initial strain rate and temperature were 1.3×10^{-4} s^{-1} and 1400°C, respectively. The specimen temperature during the mechanical test was measured by a Pt-PtRh thermocouple attached to each specimen and kept to within ±1°C.

2.3. Microstructure characterization

Microstructure of the present materials was observed by a scanning electron microscopy (SEM) and a transmission electron microscopy (TEM). An average grain size in the present materials was estimated by the linear intercept method using SEM photograph. TEM specimens were prepared using standard techniques involving mechanical grinding to a thickness of 0.1 mm, dimpling to a thickness of 20 μm and ion beam milling to electron transparency at about 4 kV. For further analysis on the grain boundaries in Al_2O_3 and TZP, high-resolution electron microscopy (HRTEM) observations were performed by using Hitachi H-9000NAR and Topcon 002BF field emission microscope. An energy-dispersive X-ray spectroscopy (EDS) analysis was carried out with Noran Voyager system attached to the Topcon microscope with the probe size of 1 nm. Atomic content of doped cation was quantitatively estimated from its Kα peak based on the thin-foil criterion [12].

2.4. Molecular orbital calculation

In order to make clear the origin of the dopant effect, chemical bonding state in cation-doped Al_2O_3 and TZP was examined by a first-principle molecular orbital calculation using the DV-Xα method [13]. In the DV-Xα method, numerical atomic orbitals obtained by solving the Schrödinger equation for atoms were used as the basic function. Therefore, the Hamiltonian and overlap matrices can be evaluated as weighted sums of integrated values at an arbitrary point in a cluster for all kinds of elements, instead of the conventional Rayleigh-Ritz method. The Mulliken population analysis provides an orbital population, the sum of which is regarded as an effective net charge (NC) as a measure of ionic valence for each cation or anion. The model clusters used were $[Al_5O_{21}]^{-27}$ for Al_2O_3 and $[Zr_{18}Y_4O_{86}]^{-88}$ for TZP. The dopant cations are substituted at Al^{3+} or Zr^{4+} cation site as a first approximation, and anion or cation vacancies were introduced to maintain electronic neutrality in the clusters.

3. Results and discussions

3.1. Small dopant effect on the high temperature creep in Al_2O_3

In case that grain boundary diffusion dominates the high temperature creep in Al_2O_3, the creep rate in Al_2O_3 is highly suppressed by $LuO_{1.5}$-doping. Fig. 1 shows the creep curves in undoped and 0.02 mol% $LuO_{1.5}$-doped Al_2O_3 at 1300°C and the applied stress of 50 MPa. The average grain size in the materials are about 5 μm. The creep deformation in Al_2O_3 is suppressed by 0.02 mol% $LuO_{1.5}$-doping. Because grain growth during creep deformation at 1300°C was negligible in Lu-doped Al_2O_3, the retarded creep rate cannot be explained from the grain size effect. It has been confirmed that the creep rate in undoped Al_2O_3 with the grain size of 5 μm exhibit the stress exponent of about 1; this result is consistent with deformation mechanism map in Al_2O_3 proposed by Heuer *et al.* [14]. Moreover, the experimental data in undoped Al_2O_3 are in good agreement with the theoretical value of Coble creep rate [15]. The dominant deformation mechanism in the undoped Al_2O_3 is probably grain boundary diffusional creep, and $LuO_{1.5}$-doping must suppress the grain boundary diffusion in Al_2O_3.

Fig. 2 shows Lu-doping dependence on the creep rate in Al_2O_3 at 1250°C and the applied stress of 50 MPa. In this figure, the steady-state creep rate in 0.02, 0.1, 0.2 or 0.4 mol% $LuO_{1.5}$-doped Al_2O_3 is plotted against $LuO_{1.5}$-doping amount, and the average grain size of undoped and Lu-doped Al_2O_3 is about 1 μm. As shown in Fig. 2, the creep rate is rapidly decreased with

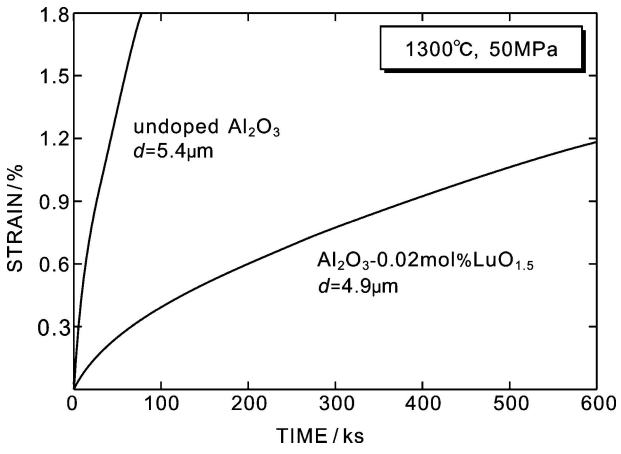

Figure 1 Creep curves in undoped Al_2O_3 and 0.02 mol% $LuO_{1.5}$-doped Al_2O_3 with a grain size of about 5 μm at 1300°C and the applied stress of 50 MPa.

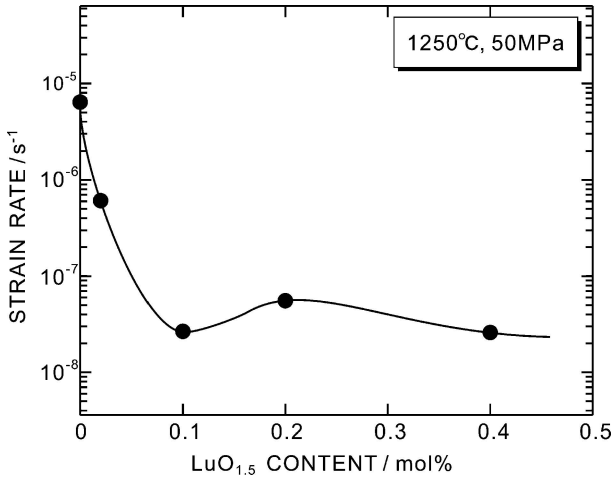

Figure 2 Steady-state creep rate in undoped and 0.02–0.4 mol% $LuO_{1.5}$-doped Al_2O_3 at 1250°C and the applied stress of 50 MPa.

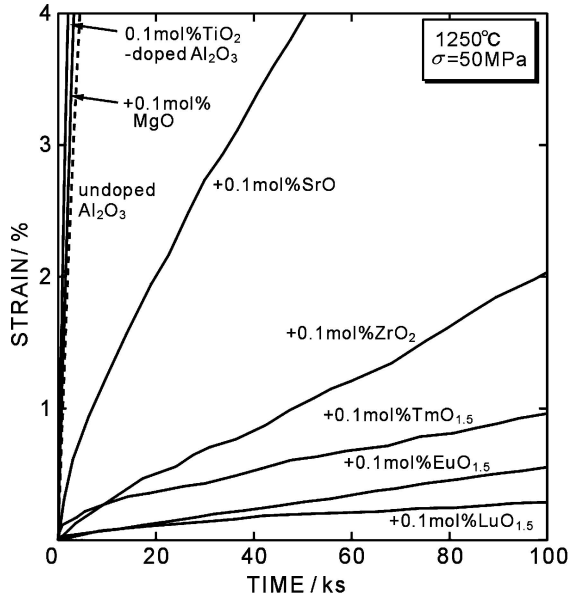

Figure 3 Creep curves in undoped Al_2O_3 and 0.1 mol% cation-doped Al_2O_3 at 1250°C and the applied stress of 50 MPa.

increasing the Lu-doping; the creep rate in 0.1 mol% Lu-doped Al_2O_3 is about 200 times lower than that in undoped Al_2O_3. However, the doping effect levels off over 0.2 mol%. In 0.4 mol% $LuO_{1.5}$-doped Al_2O_3, dispersion of second phase particles was observed by conventional TEM; the second phase is supposed to be $Al_5Lu_3O_{12}$ from the phase diagram of Al_2O_3-Lu_2O_3 system [16]. It is interesting to note that the effect of the second phase particles dispersion is minor in comparison with very small amount of Lu-doping, as well as ZrO_2-doped Al_2O_3 [4].

Fig. 3 shows the creep curves in high-purity $Al_2O_3$and various kinds of oxide-doped Al_2O_3 at 1250°C and the applied stress of 50 MPa [4, 17, 18]. The dopant content is 0.1 mol%, and the grain size is controlled to be about 1 μm in each material. In spite of the limited dopant content, the creep rate is sensitively affected by the doping; the creep rate in Al_2O_3 is retarded by SrO, ZrO_2 or lanthanoid oxide-doping, but is accelerated by MgO or TiO_2-doping. Since the high temperature creep in fine-grained Al_2O_3 is rate-controlled by the grain boundary diffusion [19–21], the difference in the creep rate is probably attributed to a change in the grain boundary diffusivity due to the cation-doping; Sr^{2+}, Zr^{4+} and lanthanoid cation-doping reduces, and Mg^{2+} or Ti^{4+}-doping enhances the grain boundary diffusion in Al_2O_3.

Concerning the mechanism of the dopant effects, a couple of ideas have been proposed so far [6, 22]. The major idea attributed the effects to ionic sizes of the dopant cations [6]. However, recent systematic studies for the lanthanoid doped Al_2O_3 revealed that the reduction in the creep rate is not in the same order as increasing ionic size of the dopant cation [17,18]. This fact indicates that the dopant effect is not so simple and cannot be explained solely from the ionic sizes.

3.2. Superplasticity in cation-doped TZP

The dopant effect on the superplastic behavior has been systematically investigated in 3Y-TZP doped with 0.2 mol% of cation. Fig. 4 shows the stress-strain curves in 3Y-TZP and 0.2 mol% BaO, $AlO_{1.5}$, $NdO_{1.5}$, SiO_2, TiO_2 or GeO_2-doped 3Y-TZP at 1400°C and an initial strain rate of 1.3×10^{-4} s^{-1} [10]. An average grain size of about 0.4–0.5 μm and a bulk density of more than 99% for theoretical density were obtained in each sample. The specimens deformed plastically and there was no necking observed at the time of failure. Superplastic behavior in 3Y-TZP is changed by 0.2 mol% cation doping; the flow stress in TZP is increased by Nd or Ba-doping, but is reduced by Si or Al-doping. On the other hand, the tensile ductility is enhanced by Si or Al-doping.

Fig. 5 shows the stress-strain curves in 3Y-TZP and 0.2–3 mol% GeO_2-doped 3Y-TZP at 1400°C and the initial strain rate of 1.3×10^{-4} s^{-1} [23]. The elongation to failure of about 440% was achieved by 2 mol% GeO_2-doping at the testing condition. However, the elongation to failure increases very little with increasing the GeO_2 content from 2 to 3 mol%. On the other hand, the flow stress decreases with increasing the GeO_2 addition up to 1 mol%, but levels off over the doping level of 2 mol%. It has been pointed out that

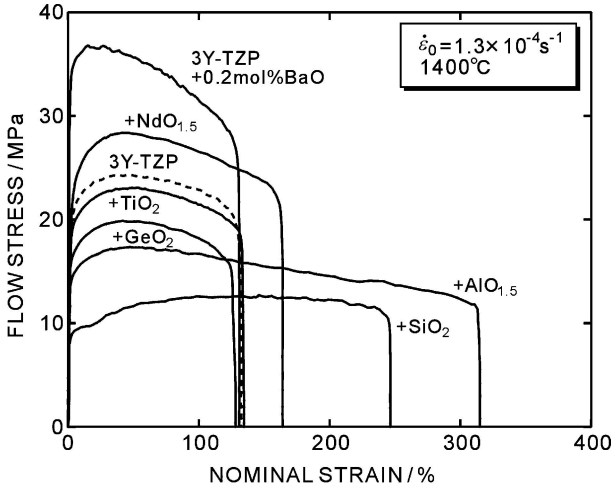

Figure 4 Stress-strain curves in 3Y-TZP and 0.2 mol% oxide-doped 3Y-TZP at 1400°C and an initial strain rate of 1.3×10^{-4} s^{-1}.

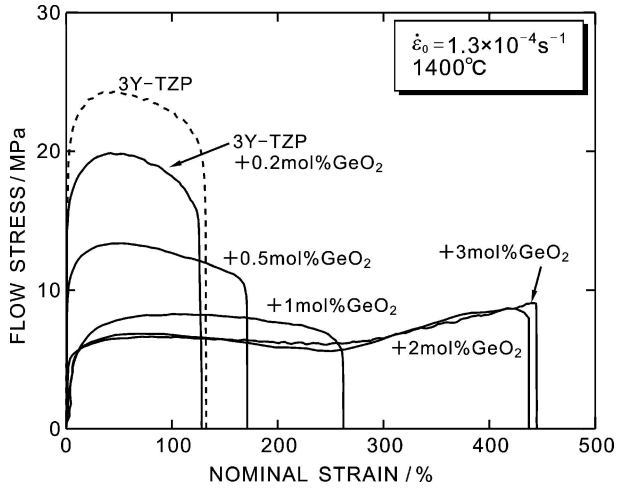

Figure 5 Stress-strain curves in 3Y-TZP and 0.2–3 mol% GeO_2-doped 3Y-TZP at 1400°C and an initial strain rate of 1.3×10^{-4} s^{-1}.

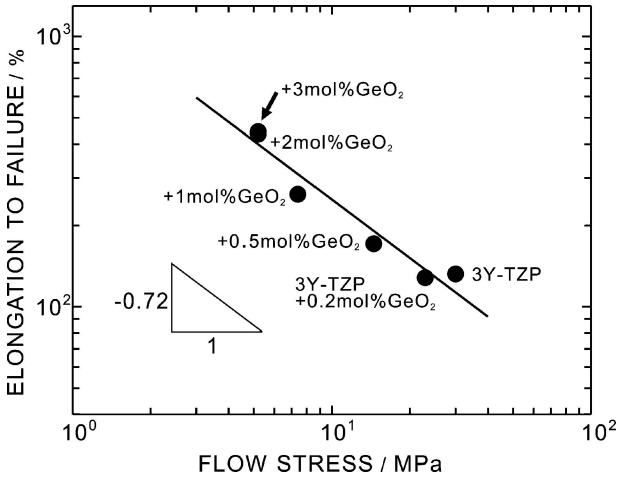

Figure 6 A logarithmic plot of elongation to failure versus 10% flow stress in 0.2–3 mol% GeO_2-doped 3Y-TZP.

the elongation to failure in superplastic ceramics is described by a function of the Zener-Hollomon parameter (Z-H parameter) of $\dot{\varepsilon}\exp(Q/RT)$; the lower Z-H parameter provides a higher value of the elongation to failure [24]. Since the Z-H parameter is proportional to the flow stress for a constant grain size, the flow stress is an important parameter for the tensile ductility in superplastic ceramics. This elongation-stress rule is satisfied over a fairly wide temperature and strain rate range [24]. Fig. 6 shows a logarithmic plot of the elongation to failure versus 10% flow stress in the present materials. The flow stress is converted to the value for a grain size of 0.5 μm using the strain rate sensitivity times the grain size exponent $mp = 1$. As shown in Fig. 6, the elongation to failure tends to increase with the decreasing flow stress. The line in Fig. 6 was given by the least-squares method, and the slope of the line was about –0.72, which is close to the predicted value of –0.66 [24]. The improved tensile ductility in GeO_2-doped 3Y-TZP can be explained based on the reduced flow stress. Therefore, Ge-doping dependence on the elongation to failure can be attributed to the leveling off behavior of the flow stress.

The GeO_2-doping dependence on the flow stress in TZP indicates that the high temperature plastic flow in TZP is very sensitive to the small levels of doping by cations as well as in fine-grained Al_2O_3. It is speculated that dopant effect on the superplasticity in TZP is attributed to difference in the grain boundary diffusivity. However, the rate-controlling mechanism for the superplastic flow in TZP is not well understood; the accommodation process for the superplastic flow is explained from either the grain boundary diffusion [25] or the lattice diffusion [8, 26]. In order to reveal the origin of the dopant effect on the high temperature plastic flow in Al_2O_3 and TZP, the microstructure of the grain boundaries were examined in detail.

3.3. Microstructure analysis in oxide ceramics

Fig. 7 shows a HRTEM image of a grain boundary in 0.1 mol% $LuO_{1.5}$-doped Al_2O_3 [27]. The HRTEM image was obtained under edge-on condition; the grain boundary plane was set parallel to the incident electron beam. The two grains is directly bonded, and there is no second phase precipitation or glass phase layer along the grain boundary. EDS analysis using a probe size of 1 nm revealed that doped Lu^{3+} cations segregate along the grain boundary [5, 27]. Scanning transmission electron microscopy (STEM)-nano-probe EDS technique also revealed the grain boundary segregation of Lu. Fig. 8 shows a STEM image (a) and Lu-Kα mapping image (b) taken with the incident beam size of 1nm in 0.1 mol% $LuO_{1.5}$-doped Al_2O_3 [27]. As shown in Fig. 8b, Lu cations present almost uniformly along the grain boundaries. This fact provides the evidence of the grain boundary segregation of Lu^{3+} cations. The grain boundary segregation is also observed in other cation-doped Al_2O_3 [4, 18]. The dopant effect on the high

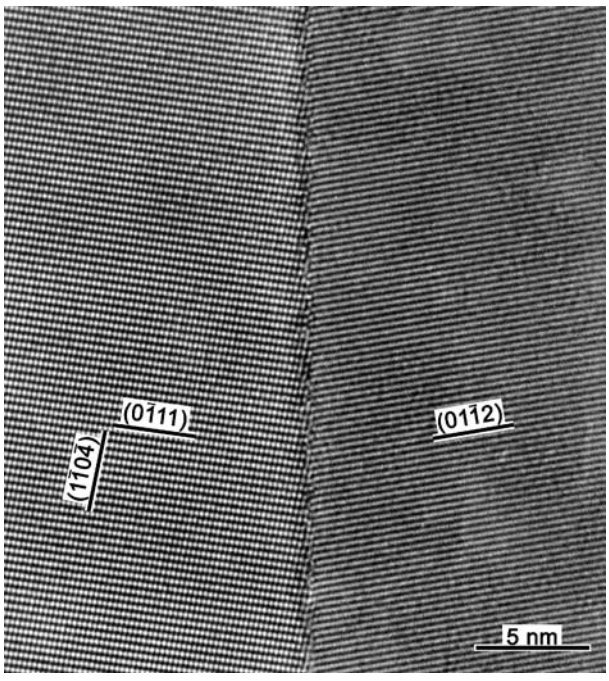

Figure 7 A high-resolution transmission electron micrograph of a grain boundary in 0.1 mol% $LuO_{1.5}$-doped Al_2O_3.

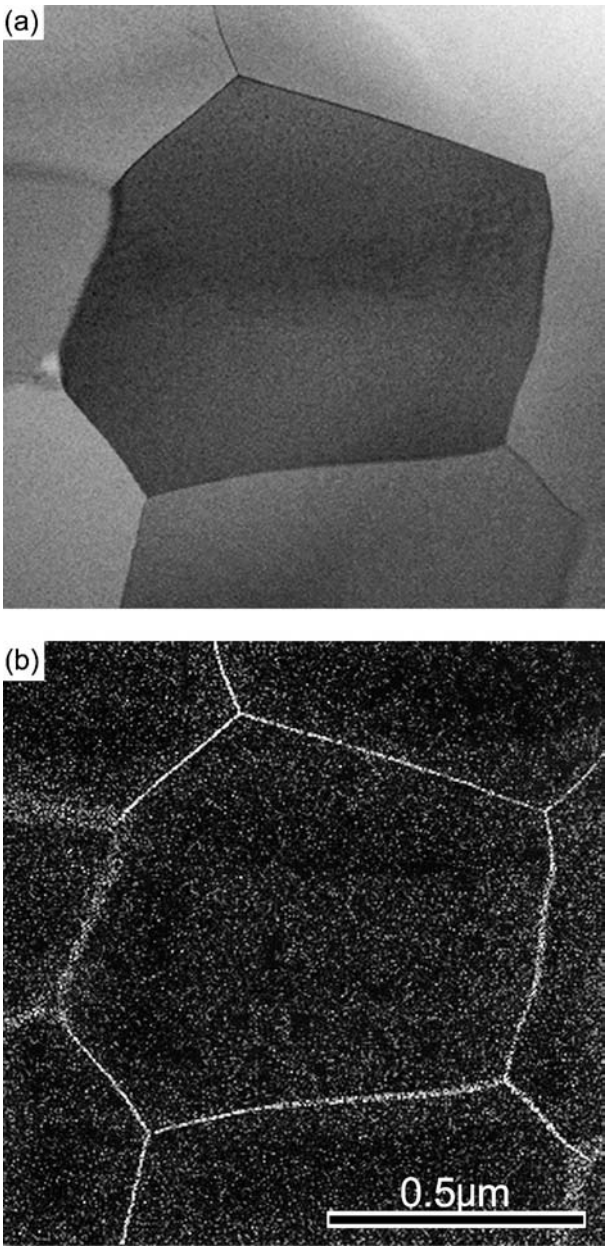

Figure 8 A scanning transmission electron microscopy (STEM) image (a) and Lu-Kα mapping image (b) obtained by STEM-EDS technique using an incident beam size of 1 nm for the grain boundaries in 0.1 mol% $LuO_{1.5}$-doped Al_2O_3.

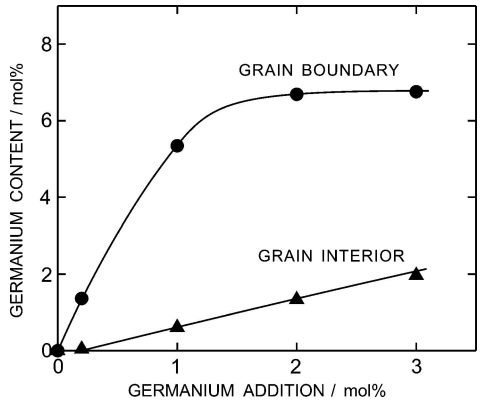

Figure 9 Atomic content of Ge^{4+} cation at the grain boundary and the grain interior against total amount of GeO_2 addition in 0.2–3 mol% GeO_2-doped 3Y-TZP.

temperature creep in Al_2O_3 is likely to result from the grain boundary segregation of doped cations. Lu-doping dependence in Fig. 2 is probably related to Lu content at the grain boundaries. In the previous paper, Y content at the grain boundary was examined in 100–1000 ppm Y_2O_3-doped Al_2O_3 [28]; the grain boundary Y content exhibited the maximum value at 500 ppm Y_2O_3-doped Al_2O_3, but leveled off over the doping amount. On the analogy of the previous data, the Lu concentration at the grain boundaries in fine-grained Al_2O_3 must become maximal value at the doping amount of 0.1 mol%, and levels off over 0.1 mol%. The Lu-doping dependence in Fig. 2 must reflect the Lu content behavior at the grain boundaries.

The segregation of the dopant cation is not a special phenomenon in Al_2O_3, but also occurs in TZP. HRTEM observation and nano-probe EDS analysis revealed that the grain boundary is a solid-solid interface without amorphous layer, and the dopant cations segregate along the grain boundaries in various kinds of cation-doped TZP [7, 10, 29]. Fig. 9 shows Ge cation content at the grain boundary and the grain interior against total amount of GeO_2 addition in 0.2–3 mol% GeO_2-doped 3Y-TZP. The Ge content was estimated from ten individual grain boundaries and grain interiors by EDS analysis using the probe size of 1nm, and the plotted data are the average values of the Ge content. The Ge^{4+} content is defined as the atomic ratio for all cations. The Ge^{4+} content at the grain boundary is larger than that in the grain interior for all specimens. This result indicates the grain boundary segregation of Ge^{4+} cations. The Ge^{4+} content at the grain boundary increases with increasing the amount of GeO_2 addition, but levels off over 2 mol% addition. Fig. 10 shows a plot of 10% flow stress against the atomic content of Ge^{4+} cation at the grain boundaries in 0.2–3 mol% GeO_2-doped TZP. The flow stress on GeO_2-doping is linearly related to the Ge^{4+} content at the grain boundary. The superplastic flow stress in TZP is dominated by chemical composition in the grain boundary. The grain boundary segregation of the dopant cation probably affects the grain boundary diffusion in TZP, and hence the small levels of doping by cations influence

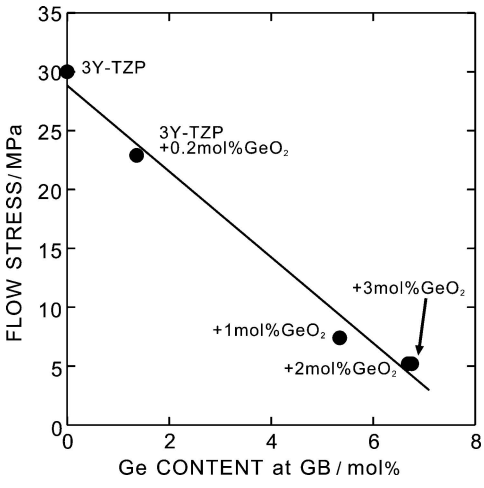

Figure 10 A plot of 10% flow stress versus atomic content of Ge^{4+} cation at the grain boundary in 0.2–3 mol% GeO_2-doped 3Y-TZP.

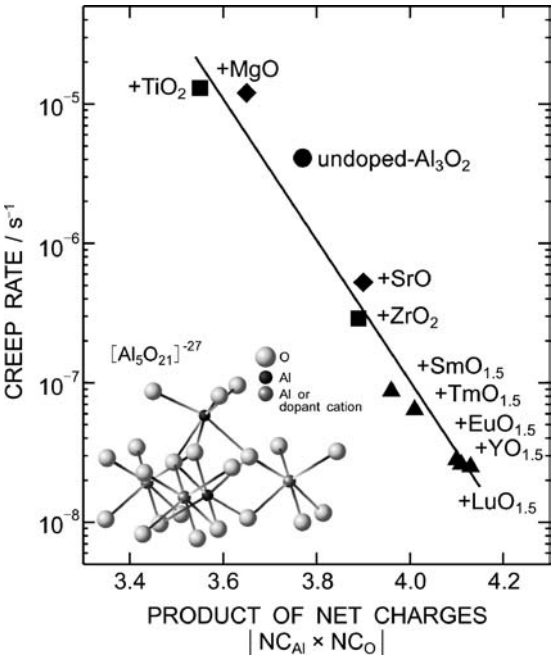

Figure 11 A plot of the creep rate in undoped and 0.1 mol% cation-doped Al_2O_3 against an absolute value of the product of Al cation net charge and O anion net charge. The model cluster of $[Al_5O_21]^{-27}$ is also shown in this figure.

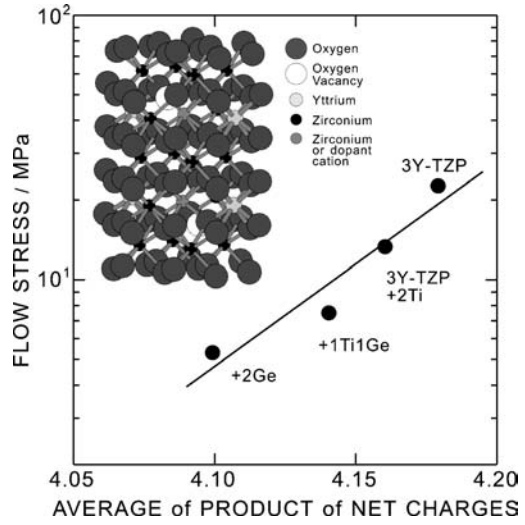

Figure 12 A plot of 10% flow stress in 2 mol%TiO_2, 2 mol%GeO_2 or (1 mol%TiO_2-1 mol%GeO_2)-doped 3Y-TZP against an average of the absolute value of the product of cation and anion net charges. The model cluster of $[Zr_{18}Y_4O_{86}]^{-88}$ is also shown in this figure.

the flow stress in 3Y-TZP as well as in fine-grained Al_2O_3.

3.4. Molecular orbital calculation

The present results indicate that the high temperature plastic flow in Al_2O_3 and TZP is strongly influenced by the chemistry in the grain boundaries. Therefore, it is necessary to examine local chemical bonding state in the grain boundaries. Our recent studies revealed that NC is a better parameter to describe the high temperature creep rate or plastic flow stress in Al_2O_3 [18]. Fig. 11 demonstrates the relationship between the high temperature creep rate in 0.1 mol% cation-doped Al_2O_3 at 1250°C and the stress of 50 MPa against an absolute value of a product of Al cation net charge (NC_{Al}) and O anion net charge (NC_O) [18]. The model cluster used for the calculation is also shown in Fig. 11. The NC_{Al} is for Al cation in the center of the cluster, and NC_O is an average value for oxygen anions surrounding the Al cation. The creep rate in cation-doped Al_2O_3 correlates well with the absolute value of the product of NC_{Al} and NC_O; the creep rate in cation-doped Al_2O_3 decreases with increasing the product of NC values. The NC product probably corresponds to ionic bond strength between Al cation and O anions, because the Coulomb's electrical attractive force between cation and anion is proportional to the product of the ionic valences [30]. Therefore, the present result suggests that the increased ionic bond strength suppresses the grain boundary diffusion in Al_2O_3.

Fig. 12 shows a relationship between the flow stress in 2 mol%TiO_2, 2 mol%GeO_2 or (1 mol%TiO_2-1 mol%GeO_2)-doped 3Y-TZP [31] and an average value of the product of NC between anion and cation in the Y-TZP model clusters. The model cluster is shown in Fig. 12; in the cluster, two Y cations are substituted for Zr cations, and oxygen vacancies are assumed to exist at the second nearest neighbor sites from Y cations. Two Ti, two Ge or (one Ti and one Ge) cations are also substituted for two Zr cation sites. The flow stress also exhibits a good correlation with the value of NC; the flow stress decreases with decreasing the value of NC. This result also suggests that TiO_2 or GeO_2-doping results in reduction of the ionicity in TZP, and the flow stress is reduced by the ionic bond reduction; the ionic bond reduction must enhance the diffusion in TZP.

The present study is probably the first trial to explain the dopant effect on the high temperature plastic flow in oxide ceramics in terms of the chemistry in the grain boundaries. The results in Figs 11 and 12 are very preliminary levels in the sense of atomic structure and chemical bonding state analysis in the grain boundaries; the model clusters were based on single crystals, not on the grain boundary structure. We will have to analyze more carefully the present results to discuss physical description of the grain boundary diffusion in terms of the chemical bonding state. More quantitative analysis on the atomic structure and the chemical bonding state in the grain boundaries in oxide ceramics will provide theoretical guiding principle to design new high-performance ceramics in the near future.

4. Conclusions

High temperature creep or superplastic flow behavior in fine-grained Al_2O_3 and TZP is sensitively affected by doping of various cations with the doping amount of 0.1–3 mol%. HRTEM-EDS and STEM-EDS technique using the incident beam size of 1nm revealed that the dopant cation tends to segregate along the grain boundaries in Al_2O_3 and TZP. The small dopant effect on the high temperature plastic flow is caused by the change in the grain boundary diffusivity due to the dopant segregation along the grian boundaries. The molecular orbital calculations suggest that ionicity correlates well

with the creep rate or the flow stress in Al_2O_3 and TZP. The ionic bonding state in the grain boundaries must be a critical factor to determine the high temperature plasticity, and probably, the grain boundary diffusivity in oxide ceramics.

Acknowledgements

The authors wish to express their gratitude to the Ministry of Education, Culture, Sports, Science and Technology and Japan Society for the Promotion of Science for the financial support by a Grant-in-Aid for Scientific Research on Priority Area and Grant-in-Aid for Encouragement of Young Scientists.

References

1. A. H. CHOKSHI and T. G. LANGDON, *Mater. Sci. Tech.* **7** (1991) 577.
2. J. WANG and R. RAJ, *Acta Metal. Mater.* **39** (1991) 2909.
3. S. LARTIGUE, L. PRIESTER, F. DUPAU, P. GRUFFEL and C. CARRY, *Mater. Sci. Eng.* **A164** (1993) 22.
4. H. YOSHIDA, K. OKADA, Y. IKUHARA and T. SAKUMA, *Phil. Mag. Lett.* **76** (1997) 9.
5. H. YOSHIDA, Y. IKUHARA and T. SAKUMA, *J. Mater. Res.* **13** (1998) 2597.
6. J. CHO, C. M. WANG, H. M. CHAN, J. M. RICKMAN and M. P. HARMER, *Acta Mater.* **47** (1999) 4197.
7. P. THAVORNITI, Y. IKUHARA and T. SAKUMA, *J. Am. Ceram. Soc.* **81** (1998) 2927.
8. M. JIMENEZ-MELEND, A. DOMINGUEZ-RODORIGUEZ and A. BRAVO-LEON, *ibid.* **81** (1998) 2761.
9. J. MIMURADA, M. NAKANO, K. SASAKI, Y. IKUHARA and T. SAKUMA, *ibid.* **84** (2001) 1817.
10. K. NAKATANI, H. NAGAYAMA, H. YOSHIDA, T. YAMAMOTO and T. SAKUMA, *Scripta Mater.* **49** (2003) 791.
11. Y. SAKKA, T. ISHII, T. S. SUZUKI, K. MORITA and K. HIRAGA, *J. Euro. Ceram. Soc.* **24** (2004) 449.
12. D. B. WILLIAMS and C. B. CARTER, in "Transmission Electron Microscopy, IV: Spectroscopy" (Plenum Press, NY, 1996) p. 599.
13. H. ADACHI, M. TSUKADA and C. SATOKO, *J. Phys. Soc. Jpn.* **45** (1978) 875.
14. A. H. HEUER, N. J. TIGHE and R. M. CANNON, *J. Am. Ceram. Soc.* **63** (1980) 53.
15. H. YOSHIDA, T. YAMAMOTO and T. SAKUMA, *J. Euro. Ceram. Soc.* **23** (2003) 1795.
16. P. WU and A. D. PELTON, *J. Alloys Coump.* **179** (1992) 259.
17. H. YOSHIDA, Y. IKUHARA and T. SAKUMA, *Phil. Mag. Lett.* **79** (1999) 249.
18. *Idem.*, *Acta Mater.* **50** (2002) 2955.
19. R. M. CANNON and R. L. COBLE, in "Deformation of Ceramic Materials," edited by R. C. Bradt and R. E. Tressler (Plenum Press, 1974) p. 61.
20. T. G. LANGDON and F. A. MOHAMED, *J. Mater. Sci.* **13** (1978) 473.
21. R. M. CANNON, W. H. RHODES and A. H. HEUER, *J. Am. Ceram. Soc.* **63** (1980) 46.
22. W. SWIATNICKI, S. LARTIGUE-KORINEK and J. Y. LAVAL, *Acta Metal. Mater.* **43** (1995) 795.
23. K. NAKATANI, H. NAGAYAMA, H. YOSHIDA, T. YAMAMOTO and T. SAKUMA, *Mater. Trans.*, **45** (2004) 2569.
24. W.-J. KIM, J. WOLFENSTINE and O. D. SHERBY, *Acta Metal. Mater.* **39** (1991) 199.
25. Y. MA and T. G. LANGDON, *Mater. Sci. Eng.* **A168** (1993) 225.
26. K. MORITA and K. HIRAGA, *Acta Mater.* **50** (2002) 1075.
27. H. YOSHIDA, Y. IKUHARA, T. SAKUMA, M. SAKURAI and E. MATSUBARA, *Phil. Mag.* **84** (2004) 865.
28. C. M. WANG, G. S. CARGILL, H. M. CHAN and M. P. HARMER, *Acta Mater.* **48** (2000) 2579.
29. Y. IKUHARA, P. THAVORNITI and T. SAKUMA, *ibid.* **45** (1997) 5275.
30. W. D. KINGERY, H. K. BOWEN and D. R. UHLMAN, in "Introduction to Ceramics" (John Wiley and Sons, NY, 1976) p. 41.
31. K. SASAKI, M. NAKANO, J. MIMURADA, Y. IKUHARA and T. SAKUMA, *Mater. Sci. Forum* **357–359** (2001) 129.

Received 9 September 2004
and accepted 31 January 2005